Decreasing spatial dependence in extreme snowfall in the French Alps since 1958 under climate change

G. Nicolet, Nicolas Eckert, Samuel Morin, J. Blanchet

AGU PUBLICATIONS

JGR

Journal of Geophysical Research: Atmospheres

RESEARCH ARTICLE
10.1002/2016JD025427

Key Points:
- Innovative data-based approach to highlight changes in the spatial dependence structure of geophysical extremes
- Evidence of a significant decreasing trend in the spatial dependence of snowfall extremes over 55 years
- Strong correlation between this trend and a decrease in both the snow rain ratio and the intensity of extreme snowfall

Correspondence to:
G. Nicolet,
gilles.nicolet@irstea.fr

Citation:
Nicolet, G., N. Eckert, S. Morin, and J. Blanchet (2016), Decreasing spatial dependence in extreme snowfall in the French Alps since 1958 under climate change, *J. Geophys. Res. Atmos.*, *121*, 8297–8310, doi:10.1002/2016JD025427.

Received 31 MAY 2016
Accepted 7 JUL 2016
Accepted article online 13 JUL 2016
Published online 25 JUL 2016

Decreasing spatial dependence in extreme snowfall in the French Alps since 1958 under climate change

G. Nicolet[1,2], N. Eckert[1], S. Morin[2], and J. Blanchet[3]

[1]Université Grenoble Alpes, Irstea, UR ETGR, St-Martin-d'Hères, France, [2]Météo-France—CNRS, CNRM, UMR 3589, CEN, Grenoble, France, [3]Université Grenoble Alpes, CNRS, LTHE, Grenoble, France

Abstract Whereas changes in magnitude of geophysical extremes under climate change have received significant attention, potential concomitant changes in spatial dependence structures have remained unexplored so far. Here we provide first evidence of such an effect, highlighting a significant trend in the spatial dependence structure of snowfall extremes in the French Alps at decadal time scale. Specifically, we process a comprehensive data set of winter maximum snowfall from all over the French Alps collected in 90 stations from 1958 to 2012. We estimate extremal dependence over 20 year moving estimation windows taking into account possible anisotropy potentially related to orographic effects and/or patterns in atmospheric flows. For each window, we derive a range representing the distance above which extremes are almost independent. We show that snowfall extremes tended to become less spatially dependent over time, with the dependence range reduced roughly by half during the study period. We demonstrate the connection between this trend and local and synoptic climatic variables associated with the current climate change context. In details, the decreasing pattern in extremal dependence is concomitant with a trend toward less harsh winter conditions. It is attributable at first to the increase in temperature and its major control on the snow/rain partitioning. Yet a magnitude effect, with less dependent extremes due to a decrease in intensity of precipitation, also exists. Finally, we show that our results are largely insensitive to the minimal modeling assumptions necessary to our data-based approach. This robustness makes it potentially suitable for various other studies in the field of geophysical extremes.

1. Introduction

Extreme snow events are among the most important hazards in mountainous regions. Snowstorms can stop road, railway, and air traffic. Extreme snowfalls can cause overloading and collapse of buildings and flooding because of snowmelt. As for other geophysical variables such as rainfall or river discharge for which high percentiles of the distribution are key quantities, extreme value theory (EVT) [*Coles*, 2001] is a suitable framework to work with. Specifically, it is now well known that block maxima (e.g., annual) should be modeled by the so-called generalized extreme value (GEV) distribution [*Blanchet and Lehning*, 2010; *Sadovsky et al.*, 2012], allowing sound extrapolation beyond the highest observed value.

However, for better mitigating risk and/or improving scientific knowledge about the processes at play, one may be interested not only in pointwise estimates but also in assessing and using dependence between extremes (extremal dependence) of different measurement stations. For instance, a proper inference of extremal dependence may help in understanding the spatial variation of extremes. This also permits to evaluate joint exceedance probabilities at different positions in space. More recent and refined statistics from the field of multivariate EVT such as extremal dependence measures are useful to this end [*Coles et al.*, 1999; *Schlather and Tawn*, 2003; *Naveau et al.*, 2009], and some of them have already been used to evaluate dependence in extreme snowfall in Switzerland [*Blanchet et al.*, 2009].

Yet to fully cope with extremes in space, max-stable processes [*de Haan*, 1984] (which are the formal extension of multivariate EVT to infinite dimension) are even more suitable. After initial developments [*Smith*, 1990; *Schlather*, 2002], *Padoan et al.* [2010] showed how different max-stable processes could be fitted to extreme rainfall in the U.S. using composite likelihood maximization techniques. This framework was applied

by *Blanchet and Davison* [2011] to extreme snow depths in Switzerland and by *Gaume et al.* [2012, 2013] to extreme snowfall and subsequently to avalanche slab depths in the French Alps. Furthermore, it was used for extreme temperature in Korea [*Lee et al.*, 2013], for extreme wind gusts in the Netherlands [*Ribatet*, 2013], for extreme wave heights in the North Atlantic Ocean [*Raillard et al.*, 2014] and in the Gulf of Lions [*Chailan et al.*, 2014], and for extreme river discharges in the upper Danube Basin [*Asadi et al.*, 2015].

However, all the previous studies assume more or less explicitly temporal stationarity, both in the GEV distributions fitted at any location of observations and, when it is modeled, in the spatial dependence structure of extremes. This is clearly questionable in the current climate change context [*Stocker et al.*, 2013]. For instance, due to the influence of temperature on the rain/snow partitioning of precipitation, snow-related variables are particularly sensitive to the recent warming [*Falarz*, 2004; *Durand et al.*, 2009a; *Valt and Cianfarra*, 2010]. It is therefore not surprising that potential trends in extreme precipitation assessed within a proper extreme value framework [*van den Besselaar et al.*, 2013; *Westra et al.*, 2013] become all the more clear when one focuses on the sole snow phase. Significant decreasing trends were highlighted in extreme snowfall and snow depths in Switzerland by *Marty and Blanchet* [2012]. In a similar spirit, using time-dependent covariates in marginal GEV distributions and a stationary spatial dependence structure within a max-stable process model, *Shang et al.* [2011] showed a relation between extreme precipitation in California and El Niño–Southern Oscillation, whereas *Westra and Sisson* [2011] highlighted the influence of global sea surface temperature and South Oscillation Index on extreme precipitations in Australia.

To the best of our knowledge, only *Huser and Davison* [2014] tried to cope for possible temporal changes in the spatial dependence structure between extreme precipitation with a time-dependent max-stable process. To this end, they developed, in a "model-based" approach, a statistical model which explicitly represents the movement of a heavy rainfall event through time, fed by observations acquired at short time steps. The scope of the current paper is to highlight potential temporal changes at longer time scales (decades) in the spatial dependence structure of snowfall extremes using a "data-based" approach, which means that we try to make as few modeling assumptions as possible in order to give more weight to the data. In addition, we carefully test sensitivity of the few hypotheses we make. By this, we aim at making sure that the revealed change in the extremal spatial dependence structure is with no doubt of geophysical origin rather than a more or less direct consequence of modeling choices.

Specifically, we process a 56 year long data set of winter maximum snowfall from all over the French Alps focusing on the spatial dependence structure only. We estimate extremal dependence over 20 year moving estimation windows and, for each window, we derive a range representing the distance above which extremes are almost independent. We highlight a strong decrease in this range over the study period, and we investigate the connection between this trend and local and synoptic climatic variables associated with the current climate change context. Finally, we demonstrate that this decrease does not depend on the choice of the parametric model nor the way the marginal distributions (i.e., the GEV distributions computed for each station) and/or the distance between stations are evaluated.

2. Data

2.1. Winter Maximum Snowfall in the French Alps

Our data set is composed of winter maxima of 3 days cumulated snowfalls with a winter period defined from 15 November to 15 May. We choose a period of 3 days because this is the most usual time scale of winter storms in the studied region and hence is often considered in avalanche forecasting [*Bocchiola et al.*, 2006; *Eckert et al.*, 2010, 2011; *Gaume et al.*, 2012]. Daily data are available from 15 November 1958 to 15 May 2013 in the French Alps (Figure 1) through observations of precipitation done mostly manually (climatological and dedicated snow observing networks). We use all the observations whose type of precipitation (rain or snow) was registered as snow. If the indication about the phase of precipitation is missing, we retain precipitations measured when minimal daily temperature is lower than 2°. Since several locations of measurement were slightly modified during the study period, we pooled together the stations with less than 100 m difference in elevation and less than 2 km in distance in the 2-D plane. Finally, we retain the 90 stations which have at least 40 winter maximum values (computed from a moving window of 3 days) during the study period (Figure 2a). Their elevation ranges from 291 m to 2012 m (Figure 2b). Hence, the station set is a good compromise between spatial and altitudinal coverage and length of records.

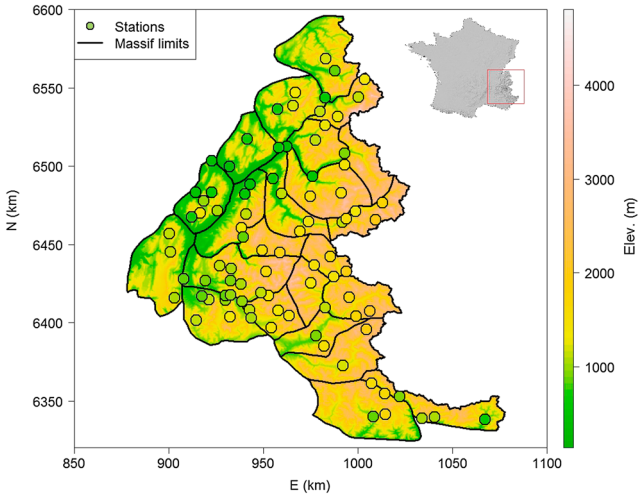

Figure 1. Study area in the southeast of France, where the 23 massifs of the French Alps are located. Lines denote massif limits, and dots denote the positions of the stations. The color code represents elevation.

2.2. Local and Synoptic Variables

In order to better understand the potential changes in extremal dependence in winter maximum snowfall, we introduce several variables that summarize the winter climate of the French Alps over the study period.

The French Alps are divided into 23 massifs (see Figure 1), which are generally assumed to be homogeneous in terms of meteorological conditions for a given elevation. In each massif, the daily snow amount and the meteorological conditions are available all over the study period as a function of elevation through reanalyses [*Durand et al.*, 2009a, 2009b]. From these reanalyses, the cumulated snowfall, mean snow water equivalent (total mass of snow per unit horizontal surface area), snow precipitation ratio (cumulated snow precipitation divided by total — snow and rain — precipitation), and mean temperature are calculated for two elevation levels (1800 m and 2400 m) for each winter and for each massif. Then, the mean of all the massif values (23 massifs for 1800 m and 21 massifs for 2400 m because the highest peaks of two massifs are below this elevation) is computed for each winter in order to have, for each variable and each winter, a single value for the entire French Alps notwithstanding the large variability of mean annual conditions [*Durand et al.*, 2009a, 2009b].

The main drivers of winter climate in the French Alps are mostly westerly fluxes coming from the North Atlantic. Thus, we also consider NAO (North Atlantic Oscillation) [*Jones et al.*, 1997; *Osborn*, 2006] and AMO (Atlantic Multidecadal Oscillation) [*Kaplan et al.*, 1998; *Enfield et al.*, 2001] indices through winter anomalies evaluated from November to April over the study period. NAO and AMO variables summarize the predominant oscillating patterns in the winter climate of the French Alps, in terms of pressure/precipitation and temperature, respectively. Rather than the commonly used detrended version of AMO [*Enfield et al.*, 2001],

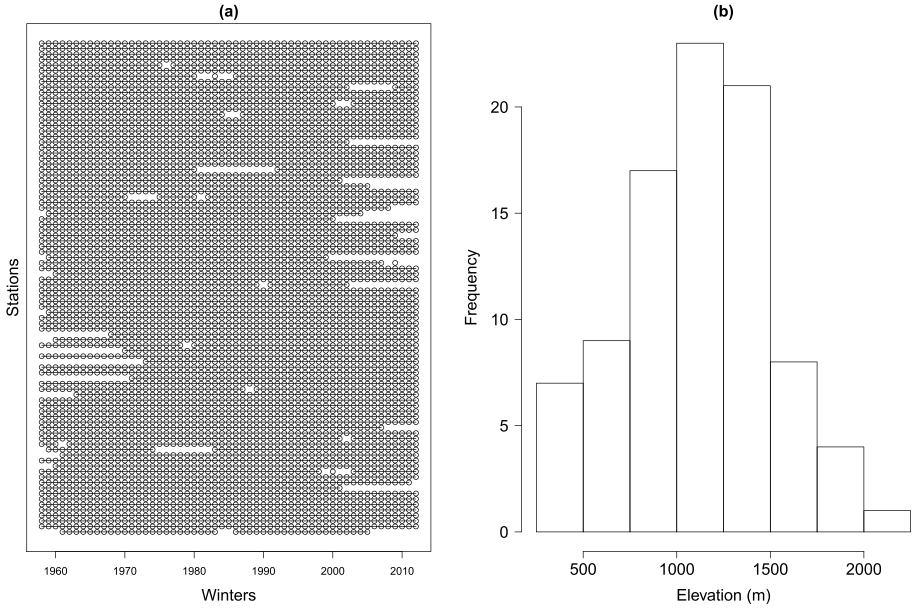

Figure 2. (a) Data availability for each station. Each line represents one station, and each point means that the winter maximum is available for that station. (b) Histogram of station elevation.

we use here the nondetrended version which includes the recent climate warming signal in addition to oscillating patterns [*Kaplan et al.*, 1998].

For consistency with the moving time windows approach of section 3.5, for each of these variables, 20 year moving averages are derived all over the study period, starting with the 1958–1977 time window and ending with the 1993–2012 time window.

3. Methods

3.1. Extreme Value Statistics in the Univariate Case and Standardization of Snowfall Maxima

Following EVT, we assume that winter maximum snowfall at a given station is GEV distributed. The cumulative distribution function $F(y; \mu(x), \sigma(x), \xi(x))$ of the GEV distribution is of the form

$$F(y; \mu(x), \sigma(x), \xi(x)) = \exp\left\{-\left[1+\xi(x)\left(\frac{y-\mu(x)}{\sigma(x)}\right)\right]^{-1/\xi(x)}\right\} \tag{1}$$

with $\mu(x)$, $\sigma(x)$, and $\xi(x)$ denoting, respectively, the location, scale, and shape parameters at position x, and y is such that $1+\xi(x)\left(\frac{y-\mu(x)}{\sigma(x)}\right)>0$. The function F is equal to 0 in the case of $\xi(x)>0$ and $y \le \mu(x)$, and equal to 1 if $\xi(x)<0$ and $y \ge \mu(x)$.

A GEV distribution is estimated for each station by likelihood maximization, giving estimates of the GEV parameters $(\mu(x), \sigma(x), \xi(x))$ at each station location x. Finally, the pointwise estimates $(\hat{\mu}(x), \hat{\sigma}(x), \hat{\xi}(x))$ are used to transform at each position x the GEV distributed snowfall maxima $\mathrm{SF}(x)$ into a unit Fréchet distributed (i.e., GEV distributed with $\mu(x)=1$, $\sigma(x)=1$ and $\xi(x)=1$) variable $Z(x)$ using the transformation

$$\mathrm{SF}(x) \mapsto Z(x) = \frac{-1}{\log\left[F\left\{\mathrm{SF}(x); \hat{\mu}(x), \hat{\sigma}(x), \hat{\xi}(x)\right\}\right]}, \tag{2}$$

where $\mathrm{SF}(x)$ is the snowfall maxima at location x and $F\{.; \hat{\mu}(x), \hat{\sigma}(x), \hat{\xi}(x)\}$ is the GEV distribution defined in (1). By doing this, we obtain a new data set of standardized winter maximum snowfall, $Z(x)$. The extremal dependence in this new data set is addressed in the current study, which is equivalent to but computationally easier than studying the extremal dependence in the original data set $\mathrm{SF}(x)$. Indeed, with the standardized data set we focus on the spatial dependence structure only and remove the effects of having different distributions for the marginal distributions, for example, due to different elevations.

In order to use the same transformation (2) for all the 20 year moving windows (see section 2.2), we first assume that the marginal distributions do not change with time. This may lead to an artificial temporal trend in the spatial dependence structure since a temporal trend in the marginal distributions may be transferred in the dependence structure. To exclude this possibility, we also assess the temporal evolution of the spatial dependence using a specific transformation (2) for each estimation window. To this end, the GEV parameters $\hat{\mu}(x)$, $\hat{\sigma}(x)$, and $\hat{\xi}(x)$ are reevaluated for each window.

3.2. Extreme Value Statistics in the Spatial Case

Let S be a space, e.g., the French Alps. Let $Z(x)$, $x \in S$ be the spatial field of standardized winter maximum snowfall in the French Alps, i.e., with every margin $Z(x)$ unit Fréchet distributed. According to spatial extreme value theory, it is appropriate to model $Z(x)$ as a max-stable process [*de Haan*, 1984; *Davison et al.*, 2012]. Every max-stable process with unit Fréchet margins holds the de Haan's spectral representation [*de Haan*, 1984]:

$$Z(x) = \sup_{i\ge 1} \eta_i W_i(x). \tag{3}$$

with $\{\eta_i\}_{i\ge1}$ the points of a Poisson process on $\mathcal{R}^+$ with intensity $\eta^{-2}d\eta$ and $\{W_i\}_{i\ge1}$ independent copies of a nonnegative process W with mean 1. Different choices for W lead to different models of max-stable processes [*Davison et al.*, 2012; *Cooley et al.*, 2012]. Every multivariate margin is given for any positions $\{x_1, \ldots, x_k\}$ by the formula

$$\mathcal{P}\left(Z(x_1) < z_1, \ldots, Z(x_k) < z_k\right) = \exp\left[-\mathbf{E}\left\{\max_{j=1,\ldots,k} \frac{W(x_j)}{z_j}\right\}\right] \qquad z_j > 0 \quad \forall j. \tag{4}$$

3.3. Extremal Coefficient and Extremal Function

To assess the extremal dependence between two unit Fréchet random variables Z_1 and Z_2, one can use the extremal coefficient θ [*Schlather and Tawn*, 2003; *Naveau et al.*, 2009] defined by

$$P\left(Z_1 < z, Z_2 < z\right) = \exp\left\{\frac{-\theta}{z}\right\} = P\left\{Z_1 < z\right\}^{\theta}, \qquad z > 0. \tag{5}$$

The extremal coefficient ranges between 1 (complete dependence) and 2 (independence). The property

$$\lim_{z\to\infty} P\left(Z_2 > z | Z_1 > z\right) = 2 - \theta \tag{6}$$

holds and means that the probability of observing extreme values of Z_2 when Z_1 takes extreme values is close to 0 when θ is near 2 and close to 1 when θ is near 1.

If $Z_1 = Z(x_1)$ and $Z_2 = Z(x_2)$ with Z a max-stable process defined by (3) and x_1 and x_2 two positions, we have from equations (4) and (5):

$$\theta(x_1, x_2) = \mathbf{E}\left[\max\left\{W(x_1), W(x_2)\right\}\right]. \tag{7}$$

Theorical expressions for θ in (7) are available for all classical max-stable processes [*Ribatet*, 2013], as functions $\theta(h)$ of the distance $h = |x_2 - x_1|$ between two positions. $\theta(h)$ represents the strength of the dependence as a function of distance and is therefore termed the extremal function.

We tried most of the currently available extremal functions. Among these, the popular Smith [*Smith*, 1990] and Schlather [*Schlather*, 2002] extremal functions are by far not flexible enough to be suitable for our case study and were discarded. In this work we consider the main other possible choice, namely, the theoretical extremal functions of the Brown-Resnick max-stable process [*Kabluchko et al.*, 2009] with a power semivariogram along with Extremal-t [*Opitz*, 2013] and Geometric Gaussian [*Davison et al.*, 2012] max-stable processes with powered exponential correlation function.

Corresponding Brown-Resnick, geometric Gaussian, and extremal-t extremal functions are respectively given by

$$\theta(h) = 2\Phi\left(\frac{\sqrt{2(h/\lambda)^{\kappa}}}{2}\right), \tag{8}$$

$$\theta(h) = 2\Phi\left(\frac{\sqrt{2\sigma^2[1-\exp\{-(h/\lambda)^{\kappa}\}]}}{2}\right) \tag{9}$$

and

$$\theta(h) = 2T_{\nu+1}\left(\sqrt{\frac{\nu+1}{1-(\exp\{-(h/\lambda)^{\kappa}\})^2}}(1-\exp\{-(h/\lambda)^{\kappa}\})\right) \tag{10}$$

with Φ and $T_{\nu+1}$, respectively, the cumulative distribution functions of the standard normal distribution and Student distribution with $\nu + 1$ degrees of freedom, $\lambda > 0$ the scale parameter, and $\kappa > 0$ the smoothness parameter. In order to keep the same degree of freedom for the three models, we fix the sill parameters $\sigma^2 = 7.7$ and $\nu = 5$ of geometric Gaussian and extremal-t extremal functions. These values impose a limit close to 1.95 to $\theta(h)$ when h tends to infinity. By doing this, we assume that extremes are still weakly dependent at two very distant locations which is a realistic hypothesis for snowfall. Therefore, each model of extremal function has two parameters: a range parameter λ and a smoothness parameter κ to be fitted on the data.

3.4. Anisotropy and Distances

In order to take into account spatial anisotropy in (8)–(10), we use three appropriate distances.

3.4.1. Modified 2-D Distance

First, we consider a modified distance in dimension 2 by using a geometric transformation of space; instead of (x_1, x_2), we compute distances using the transformed coordinates (x_1', x_2') with

$$\begin{bmatrix} x_1' \\ x_2' \end{bmatrix} = \begin{bmatrix} \cos(\alpha) & -\sin(\alpha) \\ r^{-1}\sin(\alpha) & r^{-1}\cos(\alpha) \end{bmatrix} \begin{bmatrix} x_1 \\ x_2 \end{bmatrix} \qquad r > 1 \text{ and } \alpha \in [0, \pi) \tag{11}$$

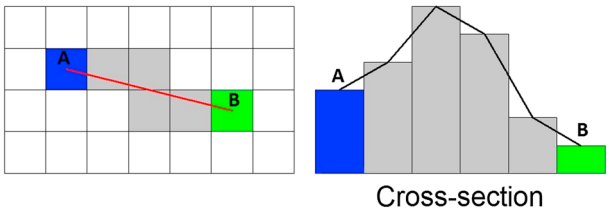

Figure 3. Example of the calculation of the crossing distance between the blue (A) pixel and the green (B) pixel. The pixels crossed by the red line linking the centers of the blue and green pixels are in grey. The crossing distance between the blue pixel and the green pixel is defined by the sum of the lengths of the black segments showed in the cross section.

where r and α denote the anisotropy ratio and angle, respectively. The angle α can be interpreted as the direction of strongest extremal dependence for pairs of stations. The parameter r controls the ratio between the direction of strongest dependence and the orthogonal direction. The 2-D Euclidean distance computed after this transformation is referred as the modified 2-D distance.

3.4.2. Modified 3-D Distance

In (11), the elevation of the standardized snowfall maxima is not taken into account. This may lead to some loss of information. Thus, we also considered the 3-D euclidean distance with the three-dimensional transformed space defined as

$$\begin{bmatrix} x_1' \\ x_2' \\ x_3' \end{bmatrix} = \begin{bmatrix} \cos(\alpha) & -\sin(\alpha) & 0 \\ r^{-1}\sin(\alpha) & r^{-1}\cos(\alpha) & 0 \\ 0 & 0 & w \end{bmatrix} \begin{bmatrix} x_1 \\ x_2 \\ x_3 \end{bmatrix} \qquad r > 1, w > 0 \text{ and } \alpha \in [0, \pi). \tag{12}$$

This modified 3-D distance is analogous to the modified 2-D distance but weighting elevation through the parameter w. This additional parameter is estimated together with r and α.

3.4.3. Crossing Distance

There exist alternatives to the space transformations (11) and (12) to take into account spatial anisotropy. Instead of considering closer the pairs of stations located along the direction of strongest extremal dependence α as done in (11) and in (12), it is also possible to compute the distances by taking into account the geographical aspects of the study area. For instance the "hydrological distance," used for river discharges, associates for each pair of locations the shortest distance in a river network [*Asadi et al.*, 2015]. Another distance, referred as the "crossing distance" in *Gottardi et al.* [2012] and more appropriate in our context, is based on the relief variations between each pair of stations. In addition to the modified 2-D distance and to the modified 3-D distance, we also consider this crossing distance. To compute it, the French Alps are divided into pixels of dimension 1×1 km, and the elevation of each pixel is given by a 1 km digital elevation model. Figure 3 shows an example of the calculation of the crossing distance between two pixels. A line linking the centers of these two pixels is drawn (red line in Figure 3), and all the pixels crossing this line are considered (in grey in Figure 3). The crossing distance is then the sum of the 3-D Euclidean distances between the pixels along this red line (represented by the black segments in the cross section of Figure 3). The Euclidean distance is applied using a weight Ω for elevation: $\sqrt{\sum \Delta x_1^2 + \Delta x_2^2 + (\Omega.\Delta x_3)^2}$. For instance, a weight $\Omega = 20$ is used for precipitation in *Gottardi et al.* [2008, 2012].

3.5. Estimation of the Extremal Dependence Over Moving Time Windows

First, we estimate the parameters (e.g., r, α, λ and κ for the modified 2-D distance) by least squares, making use of all the data together over the whole temporal period (1958–2013). Then, we hold fixed the estimations of the anisotropy parameters (e.g., r and α in the 2-D case), while the parameters λ and κ of the extremal function are reestimated on 20 year moving time windows under this anisotropic transformation.

For each estimation window (from 1958–1977 to 1993–2012) and each pair of stations, the extremal coefficient θ is estimated as follows:

$$\theta = \frac{1 + 2\nu_F}{1 - 2\nu_F} \tag{13}$$

where ν_F is the F-madogram [*Cooley et al.*, 2006; *Naveau et al.*, 2009] defined by

$$\nu_F = \frac{1}{2}\mathbf{E}\left[\left|F(Z_1) - F(Z_2)\right|\right] \tag{14}$$

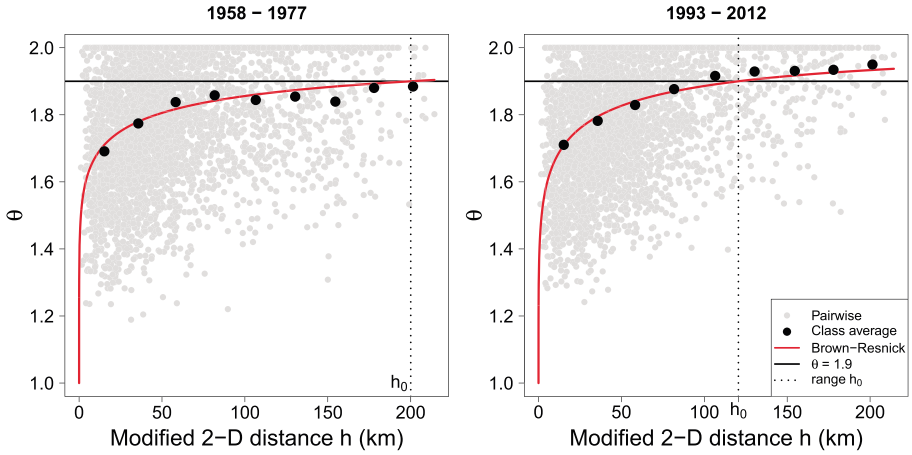

Figure 4. Extremal coefficient function for the first (1958–1977) and the last (1993–2012) estimation windows using the modified 2-D distance: madogram-based pairwise estimations of the extremal coefficient for every pairs of stations (grey dots), by distance class means (black dots), and Brown-Resnick extremal function fitted to all pairwise estimations by least squares (red curve). The range h_0 of extremal dependence (equation (15)) for the two considered time windows is $h_0 = 200$ km (1958–1977) and $h_0 = 121$ km (1993–2012), respectively.

with $F(z) = \exp(-1/z)$ the unit Fréchet cumulative distribution function. These pairwise estimations provide estimations $\hat{\theta}_h$ for all distances h between two stations (grey points in Figure 4). Then, the theoretical extremal functions (8)–(10) are fitted by least squares on the pairwise estimations $\hat{\theta}_h$, leading to $\hat{\beta} = [\hat{\lambda}, \hat{\kappa}]^T$ the vector of parameter estimates, $\Sigma = \begin{bmatrix} \text{var}(\lambda) & \text{cov}(\lambda,\kappa) \\ \text{cov}(\lambda,\kappa) & \text{var}(\kappa) \end{bmatrix}$ the variance-covariance matrix for these estimates, and $\theta(h)$, the estimated extremal function (red curve in Figure 4).

3.6. Range of Extremal Dependence

We define the range of extremal dependence as the distance h_0 such as $\theta(h_0) = 1.9$ (Figure 4). The range denotes the distance above which snowfall maxima become weakly dependent in extremes, i.e., close to independence in practice. The stronger the extremal dependence at large distances, the larger the range. Inverting (8)–(10) gives the following expressions of the range: for the Brown-Resnick extremal function

$$h_0(\beta) = h_0(\lambda,\kappa) = \lambda \left[2 \left\{ \Phi^{-1}\left(\frac{1.9}{2}\right) \right\}^2 \right]^{1/\kappa}, \tag{15}$$

for extremal-t extremal function

$$h_0(\beta) = \lambda \left[-\log \left(\frac{1 - \frac{1}{\nu+1}\left\{ T_{\nu+1}^{-1}\left(\frac{1.9}{2}\right)\right\}^2}{1 + \frac{1}{\nu+1}\left\{ T_{\nu+1}^{-1}\left(\frac{1.9}{2}\right)\right\}^2} \right) \right]^{1/\kappa}, \tag{16}$$

and for geometric Gaussian extremal function

$$h_0(\beta) = \lambda \left[-\log \left(1 - \frac{2\left\{ \Phi^{-1}\left(\frac{1.9}{2}\right)\right\}^2}{\sigma^2} \right) \right]^{1/\kappa}. \tag{17}$$

We estimate a 95% confidence interval for each estimation window by the delta method [*Cox*, 1998], propagating the standard error on $\hat{\beta}$ in equation (18). Hence, the 95% confidence interval for $h_0(\beta)$ is given by

$$\left[h_0(\hat{\beta}) - \frac{\Phi^{-1}(0.975)}{n} \nabla h_0(\hat{\beta})^T \Sigma \nabla h_0(\hat{\beta}), h_0(\hat{\beta}) + \frac{\Phi^{-1}(0.975)}{n} \nabla h_0(\hat{\beta})^T \Sigma \nabla h_0(\hat{\beta}) \right] \tag{18}$$

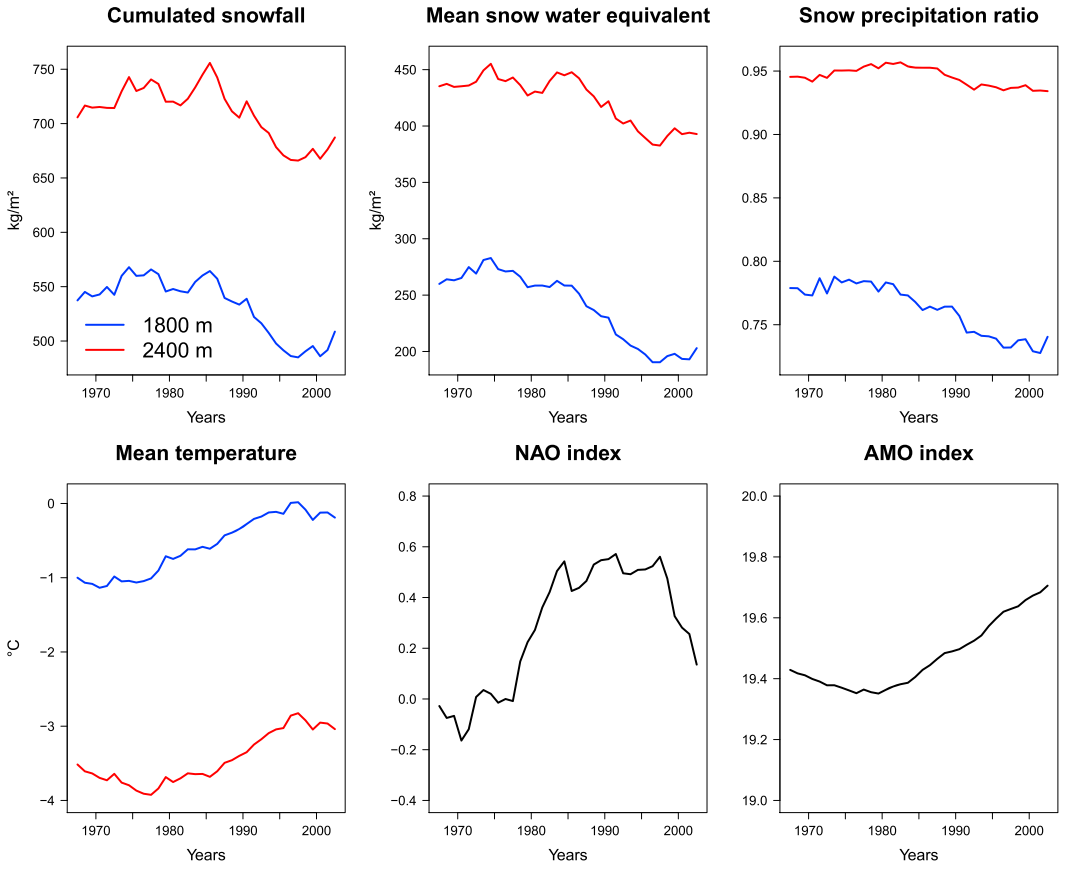

Figure 5. The 20 year moving averages of the considered variables: cumulated snowfall, mean snow water equivalent, snow precipitation ratio, and mean temperature at 1800 m (blue lines) and 2400 m (red lines) elevation levels, NAO, and AMO indexes. The *X* axis represents the center of the 20 year time window.

with ∇h_0 the gradient of h_0 with respect to β, Σ the variance-covariance matrix for the estimates and n the number of pairwise estimates of the extremal coefficient (number of pairs of stations).

4. Results and Discussion

4.1. Local and Synoptic Variables

Figure 5 shows the 20 year moving averages of the variables introduced in section 2.2. In the considered period, we observe decreases of cumulated snowfall, mean snow water equivalent, and snow precipitation ratio and increases of mean temperature, NAO and AMO. The period of strongest decrease for cumulated snowfall and mean snow water equivalent (at 1800 m and 2400 m) is from 1985 to 1997. For snow precipitation ratio, the period of strongest decrease is from 1981 to 1997 at 1800 m and from 1983 to 1993 at 2400 m. At 2400 m, the snow precipitation ratio is close to 1 during the entire study period, which means that at this elevation most of the precipitation falls as snow. Mean temperature mainly increases from 1978 to 1997 both at 1800 m and 2400 m. NAO index strongly increases from 1978 to 1985, and AMO index increases from 1978 to the end of the period of study. All of these trends come within the scope of the 1980s regime shift [*Reid et al.*, 2015].

4.2. Results Using the Entire Study Period

4.2.1. Goodness-of-Fit of the Models

Figure 6 shows the fitted Brown-Resnick, geometric Gaussian, and extremal-t extremal functions using the entire study period in the case of the modified 2-D distance. The goodness-of-fit of the models can be assessed comparing the estimated extremal functions to the class averages: a suitable extremal function should be as close as possible to the class averages. We can observe graphically or with the computation of the root-mean-square errors and the mean average errors that the three extremal functions fit well the

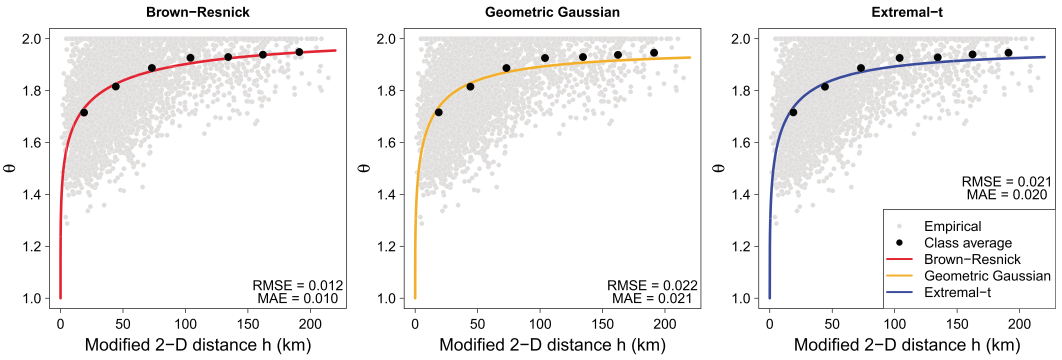

Figure 6. Estimated Brown-Resnick, geometric Gaussian, and extremal-t extremal functions in the case of the 2-D modified distance. Here models are fitted on the whole temporal period. RMSE and MAE represent, respectively, root-mean-square errors and the mean average errors between the fitted extremal functions and the class averages.

class averages. However, the Brown-Resnick extremal function seems to be slightly better, and from now we will mainly consider this extremal function.

4.2.2. Anisotropy

For the Brown-Resnick extremal function with the modified 2-D distance, we find $\hat{\alpha} = 35.84°$ (with 0° for the east and 90° for the north) and $\hat{r} = 2.78$. This anisotropy corresponds to the orientation of the main mountains and valleys in the French Alps and means that the pairs of stations located along this direction are more dependent at extreme levels. Similar observations were made in *Gaume et al.* [2013] for the French Alps with fewer observations (40 stations from 1966 to 2009), in *Blanchet and Davison* [2011] for the Swiss Alps, and in *Padoan et al.* [2010] for the Appalachians. This robust pattern may be interpreted as the effect of orography on atmospheric fluxes generating extreme precipitations. Similar estimations are found using the other extremal functions ($\hat{\alpha} = 36.57°$ and $\hat{r} = 2.78$ with geometric Gaussian extremal function and $\hat{\alpha} = 36.45°$ and $\hat{r} = 2.78$ with extremal-t extremal function) and in the 3-D distance ($\hat{\alpha} = 37.86°$, $\hat{r} = 2.76$ and $\hat{w} = 42.27$ with Brown-Resnick extremal function). The estimate of the weight parameter $\hat{w} = 42.27$ motivates the use of a weight parameter $\Omega = 40$ for the crossing distance defined in section 3.4.3.

4.3. Results Using Moving Time Windows

4.3.1. Temporal Trend

With the Brown-Resnick extremal function and the 2-D distance, we find a positive temporal trend in the extremal coefficient for distances exceeding 100 modified kilometers (Figure 7a) and, therefore, a tendency

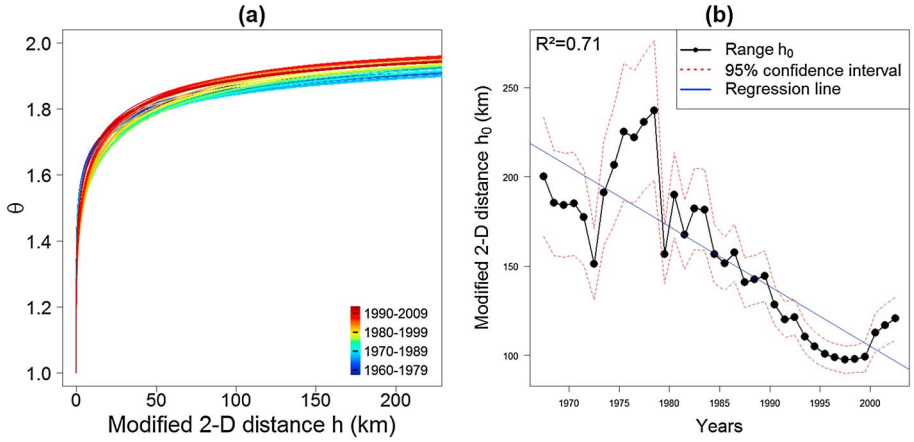

Figure 7. (a) Temporal evolution of the fitted Brown-Resnick extremal functions under the 2-D modified distance, from oldest time windows (blue curves) to the most recent ones (red curves). (b) Temporal evolution of the range of extremal dependence. The range (equation (15)) is expressed as a function of the 2-D modified distance (equation (11)). It is plotted (black dots) as a function of the center of the considered estimation window. The associated 95% confidence interval is evaluated by the delta method using equation (18). The linear fit (straight blue regression line) is made on the winter estimates (black dots).

Table 1. Correlation Table Between the Range of Dependance in Extreme Snowfall Evaluated Over 20 Year Estimation Windows and 20 Year Moving Averages of the Considered Winter Climate Variables (Section 2.2)[a]

	SF 1800	SWE 1800	T 1800	SPR 1800	SF 2400	SWE 2400	T 2400	SPR 2400	AMO	NAO	Time
Range	0.86	0.90	−0.90	0.91	0.78	0.84	−0.92	0.76	−0.86	−0.68	−0.84
SF 1800	–	0.95	−0.83	0.92	0.98	0.97	−0.97	0.88	−0.92	−0.44	−0.79
SWE 1800	–	–	−0.94	0.97	0.88	0.96	−0.98	0.83	−0.95	−0.62	−0.92
T 1800	–	–	–	−0.93	−0.72	−0.86	0.90	−0.65	0.86	0.83	0.96
SPR 1800	–	–	–	–	0.82	0.91	−0.96	0.84	−0.95	−0.60	−0.91
SF 2400	–	–	–	–	–	0.94	−0.91	0.86	−0.86	−0.30	−0.68
SWE 2400	–	–	–	–	–	–	−0.95	0.86	−0.91	−0.48	−0.83
T 2400	–	–	–	–	–	–	–	−0.88	0.96	0.56	0.86
SPR 2400	–	–	–	–	–	–	–	–	−0.87	−0.20	−0.63
AMO	–	–	–	–	–	–	–	–	–	0.45	0.88
NAO	–	–	–	–	–	–	–	–	–	–	0.73

[a]Cumulated snowfall (SF), mean snow water equivalent (SWE), mean temperature (*T*), and snow precipitation ratio (SPR), AMO, and NAO indexes. Evaluation is made with 36 values for each variable, corresponding to the 36 estimation windows from 1958–1977 to 1993–2012. The 1800 and 2400 indicate the elevation level for SF, SWE, *T*, and SPR. Time denotes the center of each estimation window.

toward less dependence in extremes at large distance in recent years. At short distances (values of the extremal function for small *h*), this decrease in strength of dependence is less visible.

There is a clear negative temporal trend in the range of extremal dependence. The correlation with time is strong (Table 1), and a linear fit of the range estimates on the center of the considered estimation window provides a determination coefficient as high as $R^2 = 0.71$ (Figure 7b). The range of extremal dependence decreased by about 3 km/yr. It reduced by almost half over the 56 year study period, from a maximum of 237 km in 1978 to around 100 km over the most recent time windows. Yet most of the decrease has been concentrated over the 1978–1997 period during which the 1980s regime shift happened [*Reid et al.*, 2015].

The corresponding 95% confidence intervals computed with the delta method (Figure 7b) show that these variations are significant. The widest confidence interval is in 1978 with a width of 79 km (95% confidence interval (198 km, 277 km)), while the width of the confidence interval is between 15 km and 25 km for the recent period.

4.3.2. Correlation With Local and Synoptic Variables

Table 1 shows that the range of extremal dependence is strongly positively correlated with the cumulated snowfall, mean snow water equivalent, and snow precipitation ratio and is strongly negatively correlated with the mean temperature, AMO, and NAO indexes. These correlations are overall slightly higher at 1800 m than at 2400 m, which is consistent with the elevation of the stations of the data set. Yet correlations remain high at 2400 m, and correlation with the mean temperature is even slightly higher at 2400 m than at 1800 m. Remember that for coherence, these correlations are based on the moving averages of the local and synoptic variables. This makes the correlations stronger than with "raw" annual values but more difficult to interpret in terms of significance level. Yet their high values and physical consistency (see hereafter) are striking.

4.3.3. Potential Climate Control on Spatial Dependence of Extreme Snowfall

The negative correlation between the range of extremal dependence and the local and synoptic temperature variables (mean temperature at the French Alps scale and AMO which refers to the temperature of the North Atlantic Ocean sea surface) shows that the dependence in extreme snowfall in the French Alps is weaker when winter temperatures are higher. Somewhat similar results were obtained very recently for extreme storms in Australia, with a reduction of their spatial extent as temperatures increases [*Wasko et al.*, 2016]. In our case of extreme snowfall, especially convincing is the concomitance between the strongest decrease in extremal dependence range (see Figure 7b) and the period of the strongest winter warming (section 4.1). Specifically, the concomitant period of strongest decrease of snow precipitation ratio from 1981 to 1997 (section 4.1) suggests that the decrease in spatial dependence of snowfall extremes could be due to a decrease of the snow precipitation ratio caused by the increase of temperature in the context of the 1980s regime shift [*Reid et al.*, 2015]. *Marty and Blanchet* [2012] suggested the same explanation for the negative temporal trends

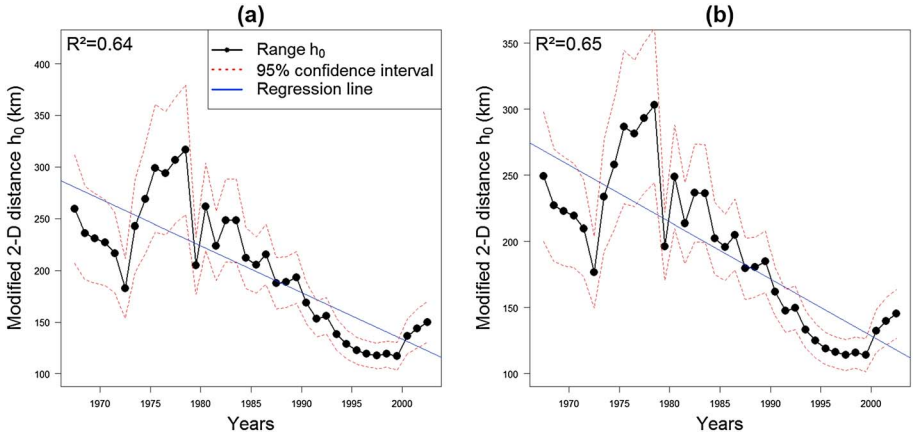

Figure 8. Same as Figure 7b with (a) geometric Gaussian extremal function and (b) extremal-t extremal function.

in extreme snowfalls in the Swiss Alps. However, it is important to note that we show here something different, since our results relate to the spatial dependence of extremes, and not to their magnitude. To the best of our knowledge, this has never been shown for any geophysical variable. Hence, the main explanation for the decrease in spatial dependence of extreme snowfall may be that the temperature increase makes these more isolated in space, at least for heavy snowfall events occurring when temperatures are not too low. In such a case, only the highest stations experience snow, while rain falls at low elevations, leading to less spatially coherent patterns in winter maxima.

Yet we cannot exclude a magnitude effect with stronger dependence in extreme snowfall in the French Alps during snowier winters. Indeed, even if the effect of snow/rain partitioning is very low at 2400 m with a snow precipitation ratio close to 1 during the entire study period (section 4.1), there is a strong positive correlation between the range and the snow variables (mean snowfall and mean snow water equivalent). This is coherent with the negative correlation with NAO, since a negative NAO anomaly is associated with harsher winter conditions widespread over the western Alps, including colder temperatures but also more intense snowfall [*López-Moreno et al.*, 2011]. Consequently, the decrease in intensity of snowfall could be an additional cause of the decrease in dependence of extreme snowfall.

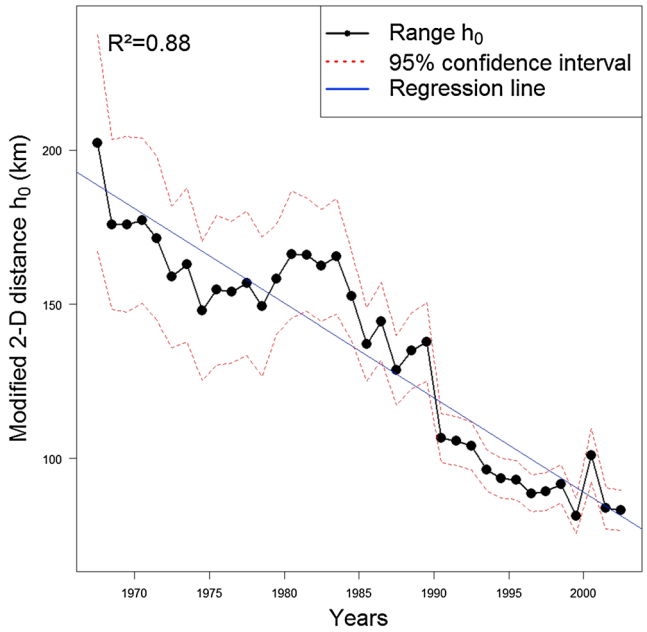

Figure 9. Same as Figure 7b when the marginal distributions are estimated and transformed into unit Fréchet on each estimation window.

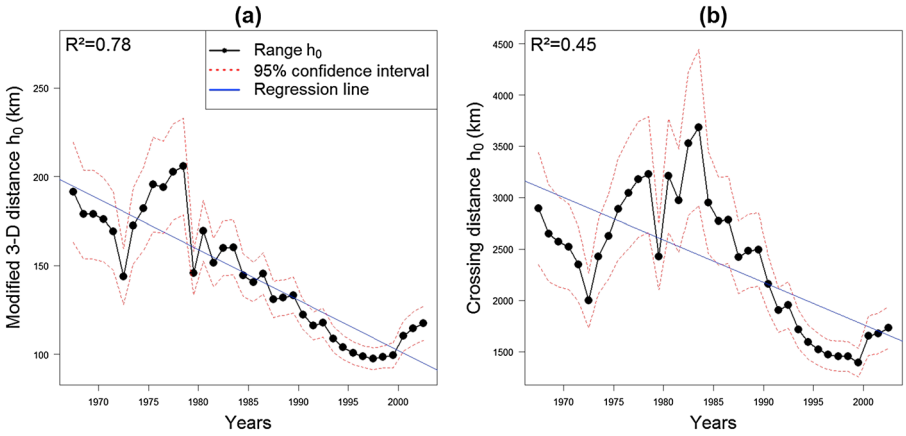

Figure 10. Same as Figure 7b with (a) modified 3-D distance and (b) crossing distance.

4.3.4. Robustness to Modeling Assumptions

Figure 8 shows that a decreasing temporal trend of the range is also found for geometric Gaussian and extremal-t extremal functions (with the 2-D modified distance), showing that this decrease is robust toward the choice of model. Figure 9 shows that when transformation into unit Fréchet involves the marginal transformations obtained on each temporal window (instead of the one obtained on the whole study period), then a similar decrease in the range is found. Finally, this decreasing temporal trend of extremal dependence is still observed under both the modified 3-D distance and the crossing distance (Figure 10). The decrease is very similar to those either with the 2-D and 3-D modified distances. Nevertheless, the decrease starts slightly later (around 1983) with the crossing distance. Yet in any case we see in Figures 8–10 that the decrease by half in the range of extremal dependence during the study period is clear, whatever the chosen hypotheses to evaluate it.

5. Conclusion and Outlook

In this paper, we show how the spatial dependence structure in extreme snowfall in the French Alps has evolved over the last decades, with a significant negative trend in the strength of extremal dependence for large distances (more than 100 km taking into account anisotropy). Specifically, we highlight a decrease of 3 km/yr of the range of extremal dependence, although this trend seems to slow down over the last years. The division by two of the range over the study period is robust with regard to how the marginal distributions are estimated, to how the way the distance between the stations is defined, and to the choice of the extremal function model, i.e., the few assumptions we had to made to conduct the study.

The decrease in the range is strongly correlated with several climate variables, at both local and synoptic scales. This suggests that climate change can have a significant impact on the spatial dependence structure of extreme snowfall. This is, to the best of our knowledge, the first evidence of such an effect.

The very strong decreasing pattern that we observe is attributable at first to the increase of temperature and to the major control exerted by temperature on the snow/rain partitioning. Yet a magnitude effect, with less dependent extremes due to a decrease in intensity of precipitation, also exists. Our result obtained on snow may therefore be of wider hydrological interest because similar trends could also exist in other variables less influenced by temperature such as rainfall.

From a statistical point of view, we did not try to fit a complete max stable model, and we chose to use a data-oriented approach. Indeed, we used time-dependent windows and took into account anisotropy, so as to highlight potential changes by fitting Brown-Resnick extremal function to pairwise estimations of extremal coefficient. Hence, even if our approach remains simpler than a model-based approach, it involves state-of-the-art tools from multivariate EVT whose inferential power we demonstrate in geophysics. This approach allows us to make minimal modeling assumptions in order to ensure the geophysical origin of the displayed temporal trend rather than a consequence of modeling choices. Our framework could therefore be useful for a variety of other studies addressing geophysical extremes in the context of climate change.

Acknowledgments
This work has been supported by a grant from LabEx OSUG@2020 (Investissements d'avenir—ANR10 LABX56). We thank hundreds of snow observers and the Météo-France staff involved in the collection and constitution of the data sets used in this study. We thank Anne-Laure Fougères (Université Lyon 1), Philippe Naveau (LSCE), Emmanuel Paquet (EDF), and Benjamin Renard (Irstea Lyon) for their advice. We thank Guillaume Evin (LTHE) and David Penot (EDF) for their help concerning the crossing distance. We thank two anonymous reviewers of a previous version of this manuscript for their useful comments and suggestions. The data for this paper are available upon request from the corresponding author (G. Nicolet, gilles.nicolet@irstea.fr).

References

Asadi, P., A. C. Davison, and S. Engelke (2015), Extremes on river networks, *Ann. Appl. Stat.*, *9*(4), 2023–2050.
Blanchet, J., and A. C. Davison (2011), Spatial modeling of extreme snow depth, *Ann. Appl. Stat.*, *5*(3), 1699–1725, doi:10.1214/11-AOAS464.
Blanchet, J., and M. Lehning (2010), Mapping snow depth return levels: Smooth spatial modeling versus station interpolation, *Hydrol. Earth Syst. Sci.*, *14*, 2527–2544, doi:10.5194/hess-14-2527-2010.
Blanchet, J., C. Marty, and M. Lehning (2009), Extreme value statistics of snowfall in the Swiss Alpine region, *Water Resour. Res.*, *45*(5), W05424, doi:10.1029/2009WR007916.
Bocchiola, D., M. Medagliani, and R. Rosso (2006), Regional snow depth frequency curves for avalanche hazard mapping in central Italian Alps, *Cold Reg. Sci. Technol.*, *46*(3), 204–221.
Chailan, R., G. Toulemonde, F. Bouchette, A. Laurent, F. Sevault, and H. Michaud (2014), Spatial assessment of extreme significant waves heights in the Gulf of Lions, *Coastal Eng. Proc.*, *1*(34), 17.
Coles, S. (2001), *An Introduction to Statistical Modeling of Extreme Values*, Springer, London.
Coles, S., J. Heffernan, and J. Tawn (1999), Dependence measures for extreme value analyses, *Extremes*, *2*(4), 339–365.
Cooley, D., P. Naveau, and P. Poncet (2006), Variograms for spatial max-stable random fields, in *Dependence in Probability and Statistics*, vol. 187, edited by P. Bertail, P. Soulier, and P. Doukhan, pp. 373–390, Springer, New York.
Cooley, D., J. Cisewski, R. J. Erhardt, S. Jeon, E. Mannshardt, B. O. Omolo, and Y. Sun (2012), A survey of spatial extremes: Measuring spatial dependence and modeling spatial effects, *Revstat*, *10*(1), 135–165.
Cox, C. (1998), Delta Method, in *Encyclopedia of Biostatistics*, vol. 2, edited by P. Armitage, and T. Colton, pp. 1125–1127, John Wiley, Chichester.
Davison, A. C., S. A. Padoan, and M. Ribatet (2012), Statistical modeling of spatial extremes, *Statist. Sci.*, *27*(2), 161–186.
de Haan, L. (1984), A spectral representation for max-stable processes, *Ann. Probab.*, *12*(4), 1194–1204.
Durand, Y., G. Giraud, M. Laternser, P. Etchevers, L. Mérindol, and B. Lesaffre (2009a), Reanalysis of 47 years of climate in the French Alps (1958–2005): Climatology and trends for snow cover, *J. Appl. Meteorol. Climatol.*, *48*(12), 2487–2512.
Durand, Y., M. Laternser, G. Giraud, P. Etchevers, B. Lesaffre, and L. Mérindol (2009b), Reanalysis of 44 yr of climate in the French Alps (1958–2002): Methodology, model validation, climatology, and trends for air temperature and precipitation, *J. Appl. Meteorol. Climatol.*, *48*(3), 429–449.
Eckert, N., C. Coleou, H. Castebrunet, M. Deschatres, G. Giraud, and J. Gaume (2010), Cross-comparison of meteorological and avalanche data for characterising avalanche cycles: The example of December 2008 in the eastern part of the French Alps, *Cold Reg. Sci. Technol.*, *64*(2), 119–136.
Eckert, N., J. Gaume, and H. Castebrunet (2011), Using spatial and spatial-extreme statistics to characterize snow avalanche cycles, *Procedia Environ. Sci.*, *7*, 224–229.
Enfield, D., A. Mestas-Nunez, and P. Trimble (2001), The Atlantic multidecadal oscillation and its relation to rainfall and river flows in the continental U.S., *Geophys. Res. Lett.*, *28*(10), 2077–2080.
Falarz, M. (2004), Variability and trends in the duration and depth of snow cover in Poland in the 20th century, *Int. J. Climatol.*, *24*(13), 1713–1727, doi:10.1002/joc.1093.
Gaume, J., G. Chambon, N. Eckert, and M. Naaim (2012), Relative influence of mechanical and meteorological factors on avalanche release depth distributions: An application to French Alps, *Geophys. Res. Lett.*, *39*, L12401, doi:10.1029/2012GL051917.
Gaume, J., N. Eckert, G. Chambon, M. Naaim, and L. Bel (2013), Mapping extreme snowfalls in the French Alps using max-stable processes, *Water Resour. Res.*, *49*(2), 1079–1098.
Gottardi, F., C. Obled, E. Paquet, and J. Gailhard (2008), Régionalisation des précipitations sur les massifs montagneux Franċais à L'aide de regressions locales et par type de temps, *Climatologie*, *5*, 7–25.
Gottardi, F., C. Obled, J. Gailhard, and E. Paquet (2012), Statistical reanalysis of precipitation fields based on ground network data and weather patterns: Application over French mountains, *J. Hydrol.*, *432*, 154–167.
Huser, R., and A. C. Davison (2014), Spacetime modelling of extreme events, *J. R. Stat. Soc. Ser. B*, *76*(2), 439–461, doi:10.1111/rssb.12035.
Jones, P. D., T. Jonsson, and D. Wheeler (1997), Extension to the North Atlantic Oscillation using early instrumental pressure observations from Gibraltar and south-west Iceland, *Int. J. Climatol.*, *17*(13), 1433–1450.
Kabluchko, Z., M. Schlather, and L. de Haan (2009), Stationary max-stable fields associated to negative definite functions, *Ann. Probab.*, *37*(5), 2042–2065.
Kaplan, A., M. Cane, Y. Kushnir, A. Clement, M. Blumenthal, and B. Rajagopalan (1998), Analyses of global sea surface temperature 1856–1991, *J. Geophys. Res.*, *103*(18), 567–18.
Lee, Y., S. Yoon, M. S. Murshed, M.-K. Kim, C. Cho, H.-J. Baek, and J.-S. Park (2013), Spatial modeling of the highest daily maximum temperature in Korea via max-stable processes, *Adv. Atmos. Sci.*, *30*(6), 1608–1620, doi:10.1007/s00376-013-2216-y.
López-Moreno, J. I., S. M. Vicente-Serrano, E. Morán-Tejeda, J. Lorenzo-Lacruz, A. Kenawy, and M. Beniston (2011), Effects of the North Atlantic Oscillation (NAO) on combined temperature and precipitation winter modes in the Mediterranean mountains: Observed relationships and projections for the 21st century, *Global Planet. Change*, *77*(1), 62–76.
Marty, C., and J. Blanchet (2012), Long-term changes in annual maximum snow depth and snowfall in Switzerland based on extreme value statistics, *Clim. Change*, *111*(3–4), 705–721, doi:10.1007/s10584-011-0159-9.
Naveau, P., A. Guillou, D. Cooley, and J. Diebolt (2009), Modelling pairwise dependence of maxima in space, *Biometrika*, *96*(1), 1–17.
Opitz, T. (2013), Extremal T processes: Elliptical domain of attraction and a spectral representation, *J. Mult. Anal.*, *122*, 409–413.
Osborn, T. J. (2006), Recent variations in the winter North Atlantic Oscillation, *Weather*, *61*(12), 353–355.
Padoan, S. A., M. Ribatet, and S. A. Sisson (2010), Likelihood-based inference for max-stable processes, *J. Am. Stat. Assoc.*, *105*(489), 263–277.
Raillard, N., P. Ailliot, and J. Yao (2014), Modeling extreme values of processes observed at irregular time steps: Application to significant wave height, *Ann. Appl. Stat.*, *8*(1), 622–647, doi:10.1214/13-AOAS711.
Reid, P. C., et al. (2015), Global impacts of the 1980s regime shift, *Global Change Biol.*, *22*, 682–703, doi:10.1111/gcb.13106.
Ribatet, M. (2013), Spatial extremes: Max-stable processes at work, *J. Soc. Fr. Stat.*, *154*(2), 156–177.
Sadovsky, Z., P. Fako, K. Mikulov, and J. Pecho (2012), Exceptional snowfalls and the assessment of accidental snow loads for structural design, *Cold Reg. Sci. Technol.*, *72*, 17–22, doi:10.1016/j.coldregions.2011.12.003.
Schlather, M. (2002), Models for stationary max-stable random fields, *Extremes*, *5*(1), 33–44.
Schlather, M., and J. A. Tawn (2003), A dependence measure for multivariate and spatial extreme values: Properties and inference, *Biometrika*, *90*(1), 139–156.
Shang, H., J. Yan, and X. Zhang (2011), El Niño–Southern Oscillation influence on winter maximum daily precipitation in California in a spatial model, *Water Resour. Res.*, *47*, W11507, doi:10.1029/2011WR010415.

Smith, R. L. (1990), Max-stable processes and spatial extremes. [Available at http://www.stat.unc.edu/postscript/rs/spatex.pdf.]
Stocker, T. F., D. Qin, G. K. Plattner, M. Tignor, S. K. Allen, J. Boschung, A. Nauels, Y. Xia, B. Bex, and B. M. Midgley (2013), *IPCC, 2013: Climate Change 2013: The Physical Science Basis. Contribution of Working Group I to the Fifth Assessment Report of the Intergovernmental Panel on Climate Change*, Cambridge Univ. Press, Cambridge, U. K., and New York.
Valt, M., and P. Cianfarra (2010), Recent snow cover variability in the Italian Alps, *Cold Reg. Sci. Technol.*, *64*(2), 146–157, doi:10.1016/j.coldregions.2010.08.008.
van den Besselaar, E. J. M., A. M. G. Klein Tank, and T. A. Buishand (2013), Trends in European precipitation extremes over 1951–2010, *Int. J. Climatol.*, *33*(12), 2682–2689, doi:10.1002/joc.3619.
Wasko, C., A. Sharma, and S. Westra (2016), Reduced spatial extent of extreme storms at higher temperatures, *Geophys. Res. Lett.*, *43*(8), 4026–4032, doi:10.1002/2016GL068509.
Westra, S., and S. A. Sisson (2011), Detection of non-stationarity in precipitation extremes using a max-stable process model, *J. Hydrol.*, *406*(1–2), 119–128, doi:10.1016/j.jhydrol.2011.06.014.
Westra, S., L. V. Alexander, and F. W. Zwiers (2013), Global increasing trends in annual maximum daily precipitation, *J. Clim.*, *26*, 3904–3918.